INORGANIC CHEMISTRY FRONTIERS

RESEARCH ARTICLE

View Article Online
View Journal | View Issue

Check for updates

Cite this: *Inorg. Chem. Front.*, 2024, **11**, 3889

Construction of a novel nickel-based MOF with accessible oxygen sites for efficient CH_4/N_2 separation†

Feifei Zhang,[a] Yuhao Tang,[a] Zhiwei Zhao,[a] Mengyue Lu,[a] Xiaoqing Wang,[a,b] Jinping Li [a,b] and Jiangfeng Yang *[a,b]

Received 22nd April 2024,
Accepted 22nd May 2024

DOI: 10.1039/d4qi01008f

rsc.li/frontiers-inorganic

Published on 23 May 2024. Downloaded on 15/9/2025 12:27:09 AM.

Enriching coal-bed methane to provide pure methane is promising and attractive. However, it is challenging due to the similar properties of CH_4 and N_2. In this work, a novel nickel-based metal–organic framework (named TUTJ-201Ni) with a high density of accessible oxygen sites was synthesized for CH_4/N_2 separation. From the structure, oxygen atoms from ligands and μ_2-hydroxyl are densely distributed on the surface of rhombic channels. Gas adsorption measurements showed that TUTJ-201Ni exhibited high CH_4 uptake over N_2. CH_4/N_2 selectivity at 298 K and 1.0 bar was calculated to be 7.2. Modeling studies indicated that the pore centers surrounded with accessible oxygen atoms are the optimal bonding sites. The stronger adsorption affinity of CH_4 can be attributed to multiple hydrogen bonding. The exceptional CH_4/N_2 separation performance of this material was further evaluated using breakthrough experiments.

1. Introduction

The shortages of traditional fossil fuels and growing environmental problems have increased the urgency for new clean energy with more environmental protection and higher calorific value. Natural gas, a fossil fuel composed mostly of methane (CH_4), is regarded as a substitute for coal and petroleum fuels due to its abundance and cleanliness.[1] Currently, the consumption of natural gas has reached 22% of the global energy consumption.[2–4] As one of the major sources of unconventional natural gas, coal-bed methane (CBM)—mainly consisting of CH_4 and N_2—is an excellent complement to conventional natural gas. Unfortunately, because of the low CH_4 content (typically ≤30%) in CBM, it is difficult to use it directly.[5] In industry, cryogenic distillation is the primary method for separating CH_4 from N_2 based on the boiling point difference between these two gases (CH_4: 112 K, N_2: 77 K).[6] However, limited by the harsh operating conditions (low temperature and high pressure), this technology is considered uneconomical and energy-intensive for CH_4 enrichment from CBM.[7]

Adsorption-based processes are a promising alternative to separate gases, owing to their high energy efficiency and intrinsic economic feasibility.[8,9] However, CH_4/N_2 separation is particularly difficult because of their similar kinetic diameters (CH_4: 3.8 Å, N_2: 3.6 Å) and comparable polarizability (CH_4: 26.0 × 10^{-25} cm^3, N_2: 17.6 × 10^{-25} cm^3).[10,11] Numerous traditional porous materials, including activated carbons, zeolites, and molecular sieves, have been developed for CH_4/N_2 separation, but they suffer from low selectivity and/or poor capacity.[12–15] Therefore, the design of new adsorbents that combine a high CH_4 selectivity and capacity is urgent.

In the past decades, metal–organic frameworks (MOFs) have received attention and shown great promise for gas separation because of their structural diversity and high tunability.[16–21] Regarding the CH_4/N_2 adsorption separation, many MOFs have been reported to fulfill this important task.[22–27] Among the diverse range of MOFs reported so far, materials containing accessible oxygen sites show high separation potential in CH_4/N_2 separation especially beneficial for improving CH_4 selectivity. For example, Bao and colleagues reported the synthesis of a squarate-based MOF, $Co_3(C_4O_4)_2(OH)_2$, benefiting from the high density of negative oxygen binding sites in the pore wall, this material exhibited a high adsorption selectivity (12.5) of CH_4 over N_2 at 298 K and 1.0 bar.[28] Similarly, Xia *et al.* reported an MOF named CAU-21-BPDC, which has a high CH_4/N_2 selectivity of 11.9 because of the strong adsorption affinity between CH_4 molecules and μ_2-oxygen atoms from metal clusters.[29] Finally, Liu *et al.* found that STAM-1 had high CH_4/N_2 selectivity (11.5 at 298 K and 1.0 bar) due to the presence of a high density of negative oxygen

[a]*Research Institute of Special Chemicals, College of Chemistry and Chemical Engineering, Taiyuan University of Technology, Taiyuan 030024, Shanxi, China. E-mail: yangjiangfeng@tyut.edu.cn*
[b]*Shanxi Key Laboratory of Gas Energy Efficient and Clean Utilization, Taiyuan 030024, Shanxi, China*

†Electronic supplementary information (ESI) available. CCDC 2345232 and 2345233. For ESI and crystallographic data in CIF or other electronic format see DOI: https://doi.org/10.1039/d4qi01008f

Published on 23 May 2024. Downloaded on 15/9/2025 12:27:09 AM.

atoms.[30] Overall, these oxygen-rich MOFs exhibit excellent CH_4/N_2 selectivity. To our knowledge, there are few studies of CH_4/N_2 separation behavior of oxygen-rich MOFs reported in the literature. Therefore, there is an urgent need to put more effort into this aspect of MOF research.

In this study, we prepared an ultramicroporous MOF, TUTJ-201Ni, which features a high density of accessible oxygen sites on the pore wall. The CH_4 and N_2 adsorption properties of TUTJ-201Ni have been characterized by isotherms, heats of adsorption (Q_{st}), and the ideal adsorbed solution theory (IAST) selectivity. Breakthrough experiments were performed to evaluate its CH_4/N_2 separation performance under dynamic conditions. Moreover, theoretical calculations combined with *in situ* infrared (IR) spectra were performed to further decipher the separation mechanism.

2. Experimental section

2.1 Materials

Nickel nitrate hexahydrate ($Ni(NO_3)_2{\cdot}6H_2O$, 99%) and 3,3′-bipyridine-5,5′-dicarboxylic acid (H_2L, 98%) were purchased from Jilin Chinese Academy of Sciences-Yanshen Technology Co., Ltd. Tetrafluoroboric acid (HBF_4, 48%) was purchased from Shanghai Aladdin Biochemical Technology Co., Ltd. *N*,*N*-Dimethylacetamide (DMA, 99%) and acetone (CH_3COCH_3, 99%) were provided by Sinopharm Chemical Reagent Co., Ltd. The above reagents were used directly without further purification. The distilled water used in the experiment was made by our laboratory.

2.2 General methods

The crystallinity of the TUTJ-201Ni powder was tested using a Bruker D8 ADVANCE X-ray diffractometer. The test was conducted using Cu-Kα (λ = 1.5418 Å) radiation, and the working voltage and current were 40 kV and 40 mA, respectively. Scanning was performed over the 2θ range of 5°–40° at 5° min^{-1}. Thermogravimetric analysis (TGA) of the samples was performed using a Netzsch STA 449 F5 (Germany) differential thermal analyzer at an airflow rate of 100 mL min^{-1}. The temperature test range was 298–1073 K, and the heating rate was 10 K min^{-1}. Scanning electron microscopy (SEM) was performed on a ZEISS Sigma 300 at an accelerating voltage of 5 kV and energy dispersive X-ray spectroscopy was carried out using a Smart EDX system equipped with X-ray mapping at an accelerating voltage of 15 kV. The IR spectra were measured using a Shimadzu FT-IR 8400s Fourier-transform (FT) IR spectrometer. X-ray photoelectron spectroscopy (XPS) was measured on a Thermo ESCALAB 250XI using a monochromatized Al Kα X-ray source, in which all of the binding energies were calibrated with reference to the C 1s peak (284.8 eV). Before the test, the samples and KBr were dried in an oven at 353 K for 2 h. CH_4 and N_2 single-component gas adsorption isotherms were measured using an APSP 2460 analyzer. The nitrogen adsorption and desorption isotherms of the samples at 77 K were obtained using an APSP 2020 analyzer. The kinetic profiles for N_2 and CH_4 adsorption were measured using an Intelligent Gravimetric Analyzer (IGA 001, Hiden, UK). The samples were activated at 423 K and 1×10^{-1} mbar for 5 h before testing.

2.3 Synthesis

Synthesis of TUTJ-201Ni. We placed 9.0 mL of DMA, 0.9 mL of H_2O, and 0.1 mL of HBF_4 (48 wt%) in a 20 mL glass vial containing $Ni(NO_3)_2{\cdot}3H_2O$ (90.0 mg, 0.37 mmol) and H_2L (30.0 mg, 0.12 mmol). The vial was sealed and placed in an oven preheated to 353 K. The solvothermal reaction took place at this temperature for 24 h. The products were collected by suction filtration and washed several times with fresh DMA and acetone.

2.4 Rietveld refinement for TUTJ-201Ni

The crystal structure data used in the refinement process were derived from the reported TUTJ-201Co crystal structure. The refinement results of TUTJ-201Ni were obtained by the Rietveld method using TOPAS software (Table S2, CCDC 2345233†).

2.5 *In situ* IR spectroscopic analysis

In situ IR spectra of adsorbed CH_4 and N_2 were obtained using a Bruker V70 equipped with an MCT detector, stainless steel high-temperature *in situ* IR cell, and KBr window. The resolution of the IR spectrum was set to 4 cm^{-1}. For the analysis, a certain amount of adsorbent powder was placed in the sample cup of the high-temperature reaction cell and the powder scraped flat. TUTJ-201Ni samples were activated at 423 K and 1×10^{-1} mbar for 5 h. During the activation process, the heating and cooling rates of the adsorbent were both 5 K min^{-1}. After the adsorbent was cooled to the test temperature, the IR spectrum of the activated sample was recorded as the background spectrum. Then, the tested gas was passed into the test system, and the IR data were collected until the adsorbent was saturated.

2.6 Breakthrough tests

In this experiment, we obtained the breakthrough curves of TUTJ-201Ni when the mixed gas flow rate was 8–16 mL min^{-1}. The prepared TUTJ-201Ni (1.2 g) particles were activated at 423 K and 1×10^{-1} mbar for 5 h and then placed in an adsorption column (∅ 4.0 mm × 100 mm) in an environment free from water. Before starting the test, the adsorption column was flushed with He gas at a flow rate of 15 mL min^{-1} and 373 K, and then the inlet gas was switched to the mixture to be tested at a total gas flow rate of 8–16 mL min^{-1}. The spectra of the gas at the outlet of the adsorption column were recorded using an online mass spectrometer (HPR-20 EGA, Hiden, detection limit 0.01%) to obtain the final breakthrough curves.

3. Results and discussion

TUTJ-201Ni was prepared from the reaction of 3,3′-bipyridine-5,5′-dicarboxylic acid and nickel nitrate hexahydrate in a

 This journal is © the Partner Organisations 2024

Published on 23 May 2024. Downloaded on 15/9/2025 12:27:09 AM.

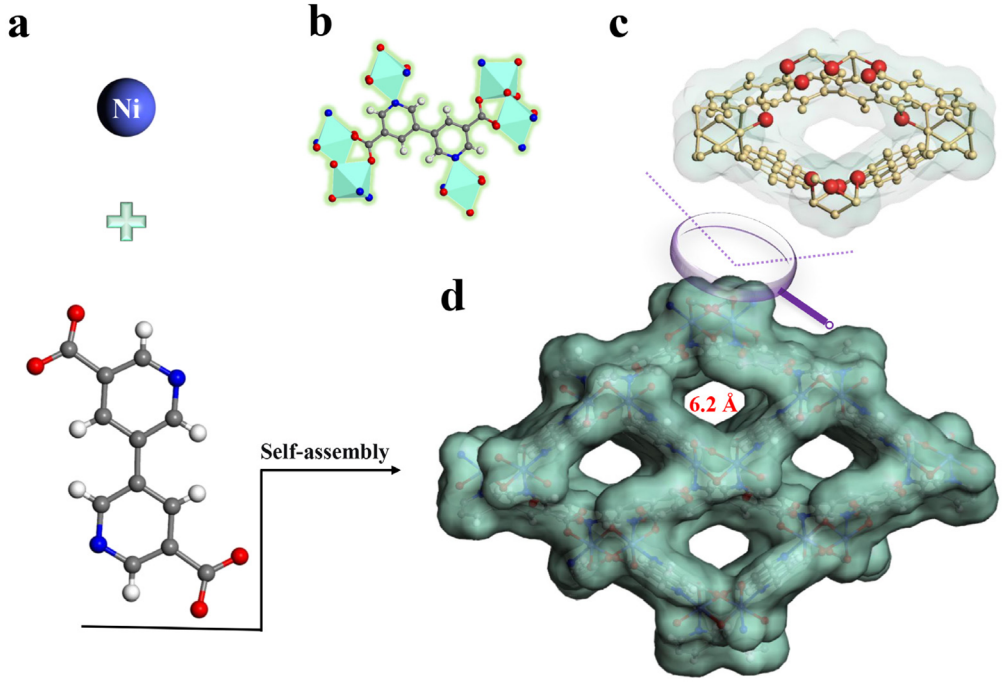

Scheme 1 Structural description of TUTJ-201Ni. (a) Framework of TUTJ-201Ni formed by nickel atoms and 3,3′-bipyridine-5,5′-dicarboxylic acid ligand. (b) Local coordination environments of the organic ligand and metal centers. (c) Pore aperture and pore chemistry of TUTJ-201Ni. (d) Crystal structure of guest-free TUTJ-201Ni, showing one-dimensional channels. Color code: C, gray; H, white; O, red; Ni, indigo; N, blue.

mixture of water and DMF at 353 K for 24 h (Scheme 1). The structure of this MOF was accurately analyzed through Rietveld refinement using TOPAS software (CCDC: 2345233†) (Fig. 1a). Like TUTJ-201Co (Table S1†), TUTJ-201Ni crystallizes in the monoclinic space group *Pbcn* (Table S2†) and possesses the formula $C_{24}H_{12}Ni_2N_4O_9$. As described in Scheme 1, the framework is formed from hydroxide groups bridging regular octahedra of nickel atoms and organic linkers. Each nickel metal center exhibits an octahedral coordination environment through connection with four oxygen atoms and two nitrogen atoms, where three oxygen atoms and two nitrogen atoms are from five different organic linkers whereas the remaining oxygen atom comes from the bridging hydroxide group. TUTJ-201Ni shows rhombic-shaped one-dimensional channels of approximately 6.2 Å along the crystallographic *b*-axis, and the pore wall was decorated by multiple oxygen sites.

As shown in Fig. 1a, the structure of TUTJ-201Ni was identified by Le Bail analysis, which shows good reliability factors (R_p = 0.0612 and R_{wp} = 0.0468), indicating that TUTJ-201Ni has an identical framework to TUTJ-201Co. As shown in Fig. 1b, SEM/EDX mapping shows that TUTJ-201Ni had spindle-shape morphology and the O elements were uniformly distributed on the crystal surface. The content of O element was further verified using XPS (Fig. 1c), one peak was detected at 530.9 eV, revealing the presence of O^{2-} ions in the framework, and the atomic ratio for O/Ni reached up to 4.85 (Table S4†). To probe the porous nature of TUTJ-201Ni, 77 K N_2 adsorption experiments were conducted (Fig. 1d). The resulting N_2 adsorption isotherms display a typical type-I behavior with a sharp increase at low relative pressures, validating its inherent microporous structures. The calculated Brunauer–Emmett–Teller (BET) surface area and pore volume were 432 $cm^2\ g^{-1}$ and 0.14 $cm^3\ g^{-1}$, respectively. The pore size distribution was further analyzed using the standard non-local density functional theory model (Fig. 1e). The observed pore size was mainly concentrated at 0.59 Å, which is in line with the theoretical value. We also investigated the thermal stability of TUTJ-201Ni using TGA and variable-temperature PXRD experiments. As shown in Fig. 1f and S6, S7,† the results show that the framework is thermally stable up to 300 °C. The exceptional stability of TUTJ-201Ni could be attributed to the robust Ni–N bonds in the framework.

Single-component isotherms of CH_4 and N_2 were measured at different temperatures up to 1.0 bar (Fig. S8†). As shown in Fig. 2a, TUTJ-201Ni shows extremely steep CH_4 adsorption isotherms at low pressure, whereas N_2 exhibits an almost linearly increasing trend. At 1.0 bar, the uptake of CH_4 reaches 19.8 $cm^3\ g^{-1}$, which is 3.9 times higher than that of N_2 (5.0 $cm^3\ g^{-1}$). This significant difference in the adsorbed amount indicates that TUTJ-201Ni has a stronger affinity for CH_4 over N_2. To evaluate the CH_4 uptake of TUTJ-201Ni, its CH_4 uptake was compared with that of other adsorbents. As shown in Table S5,† CH_4 uptake is higher than that of $Co_3(C_4O_4)_2(OH)_2$ (8.9 $cm^3\ g^{-1}$),[28] STAM-1 (14.2 $cm^3\ g^{-1}$)[30] and $Co_3(HCOO)_6$ (11.0 $cm^3\ g^{-1}$),[31] comparable to the other state-of-the-art porous materials such as SBMOF-1 (20.6 $cm^3\ g^{-1}$),[27] CAU-21-BPDC (22.2 $cm^3\ g^{-1}$)[29] and $Cu(INA)_2$ (18.6 $cm^3\ g^{-1}$).[32] To estimate further the separation performance of TUTJ-201Ni,

Published on 23 May 2024. Downloaded on 15/9/2025 12:27:09 AM.

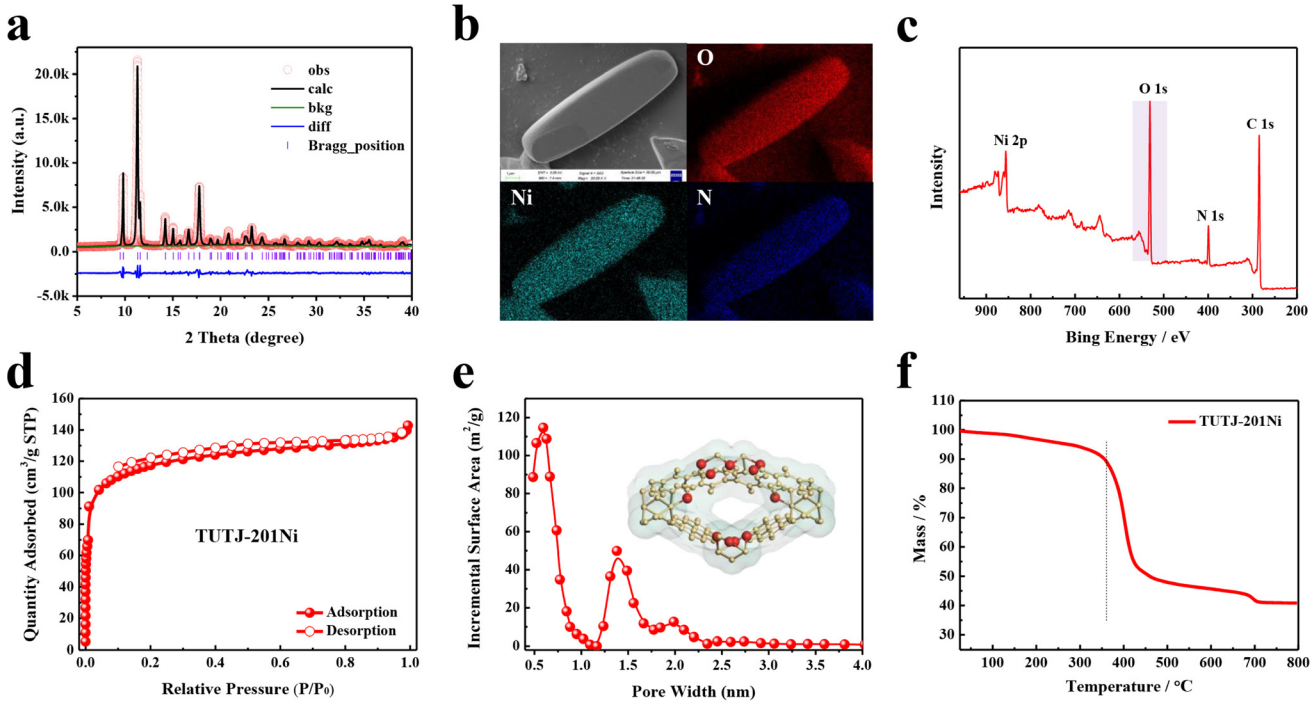

Fig. 1 (a) Rietveld-refined XRD pattern obtained for TUTJ-201Ni (R_{wp} = 6.12%, R_p = 4.68%, GOF = 2.01, a = c = 3.06 Å, b = 16.57 Å, α = 90°, β = 90°, γ = 120°). The black lines and red circles represent the experimental data and calculated values, respectively. (b) SEM/EDX mapping of TUTJ-201Ni. (c) XPS spectrum obtained for TUTJ-201Ni: O 1s spectra. (d) N_2 sorption isotherms obtained for TUTJ-201Ni at 77 K. (e) Calculated pore size distribution of TUTJ-201Ni. (f) TGA curve obtained for TUTJ-201Ni.

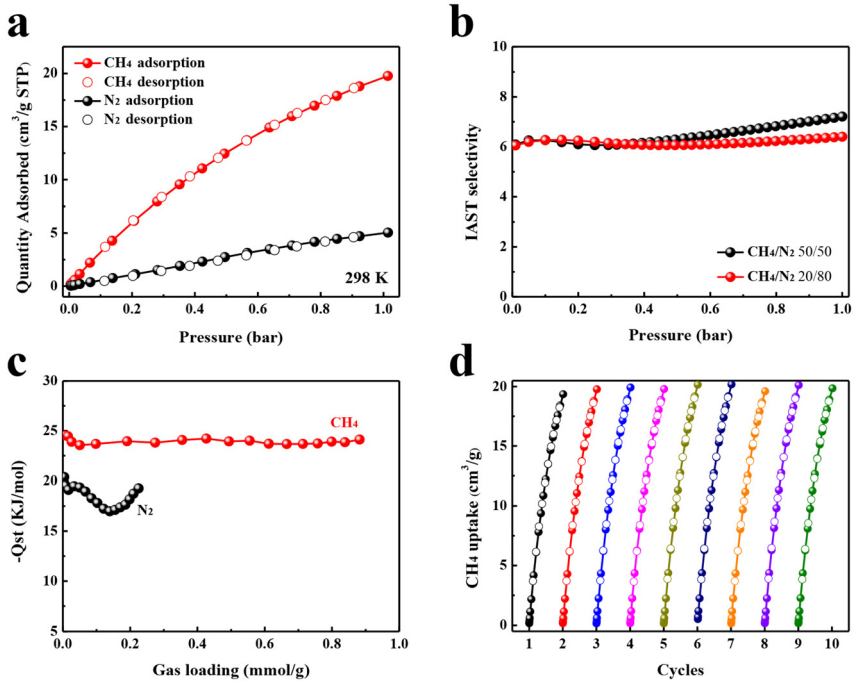

Fig. 2 (a) CH_4 and N_2 adsorption isotherms measured for TUTJ-201Ni at 298 K. (b) IAST selectivity of CH_4/N_2. (c) Q_{st} curves calculated for CH_4 and N_2 sorption. (d) The recycling performance of TUTJ-201Ni.

 This journal is © the Partner Organisations 2024

Published on 23 May 2024. Downloaded on 15/9/2025 12:27:09 AM.

the CH_4/N_2 selectivities were calculated using IAST. As displayed in Fig. 2b, the calculated CH_4/N_2 selectivity for the corresponding binary equimolar mixture in TUTJ-201Ni is up to 7.2 at 298 K and 1.0 bar. This value is comparable to a series of reported materials, including CAU-10 (7.2),[33] ZIF-94 (7.4)[34] and MOF-891 (7.8).[35] Q_{st} of CH_4 and N_2 were further calculated using the dual-site Langmuir–Freundlich model to evaluate the interactions between the adsorbents and gases (Fig. 2c). The Q_{st} values of CH_4 are in the range of 24.5–24.1 kJ mol^{-1}, which is notably higher than that of N_2 (20.2–19.2 kJ mol^{-1}) in the whole range. At zero loading, the Q_{st} of CH_4 for TUTJ-201Ni is 24.5 kJ mol^{-1}, which is significantly higher than that of most high-performance MOFs,[27,29,32] implying a strong binding interaction between CH_4 and the framework. Interestingly, we found that upon increasing the CH_4 loading, the Q_{st} value were smooth lines with almost unchanged values. This implies the energetic homogeneity of the TUTJ-201Ni surface, and a similar phenomenon was also observed in $[Co_3(C_4O_4)_2(OH)_2]$.[28] Furthermore, the nine cycles of CH_4 adsorption/desorption tests indicate that TUTJ-201Ni has excellent reproducibility (Fig. 2d), the successive adsorption/desorption cycles were measured at 298 K and a testing pressure up to 1.0 bar without a regeneration process.

For insight into the adsorption mechanism of CH_4 and N_2 in TUTJ-201Ni at the molecular level, we carried out grand canonical Monte Carlo (GCMC) simulations and density functional theory (DFT) calculations to illustrate the interactions between the framework and gases. As shown in Fig. 3a and b, the CH_4 and N_2 gas molecules both appear around the center of the rhombic pore, indicating pore centers are the most energetically favorable binding sites for both adsorbates. The density of CH_4 adsorbed in TUTJ-201Ni is obviously higher than that of N_2, which is in full agreement with their adsorption capacities. DFT calculations were thereafter carried out to directly visualize the locations of CH_4/N_2 within TUTJ-201Ni. As revealed in Fig. 3c, the CH_4 molecule is preferentially adsorbed at the center of the MOF pore, where it forms three C–H···O hydrogen-bonding interactions with the two nearby uncoordinated carboxylate oxygen atoms and one μ_2-hydroxyl oxygen atom, with close interaction distances ranging from 3.25 to 3.67 Å. By contrast, the N_2 molecule is oriented parallel to the *c*-axis in the channels and interacts with the framework through weak van der Waals forces with N≡N···O distances of approximately 3.36 and 3.98 Å (Fig. 3d). Obviously, the average distance between a CH_4 molecule and the framework is shorter than that for N_2, indicating a stronger adsorption affinity of TUTJ-201Ni for CH_4 over N_2. The calculated binding energies for CH_4 and N_2 are respectively 28.6 and 23.0 kJ mol^{-1}, which is in accordance with the experimental findings.

In situ IR spectroscopic measurements were carried out to probe further the interaction of CH_4 within TUTJ-201Ni. Fig. 4 presents the change of stretching bands upon CH_4 loading. Two distinct stretching bands at 1303 and 3014 cm^{-1} are observed, which are attributed to the δ(C–H) and ν_s(C–H) stretching bands, respectively. This observation proved the strong interaction between CH_4 molecules and the framework.[25] With the adsorption of the CH_4 on TUTJ-201Ni, the intensity of the stretching band significantly increased. This may be attributed to the high gas adsorption capacity of this material.

To evaluate the feasibility of TUTJ-201Ni for a practical CH_4/N_2 separation, experimental breakthrough studies were

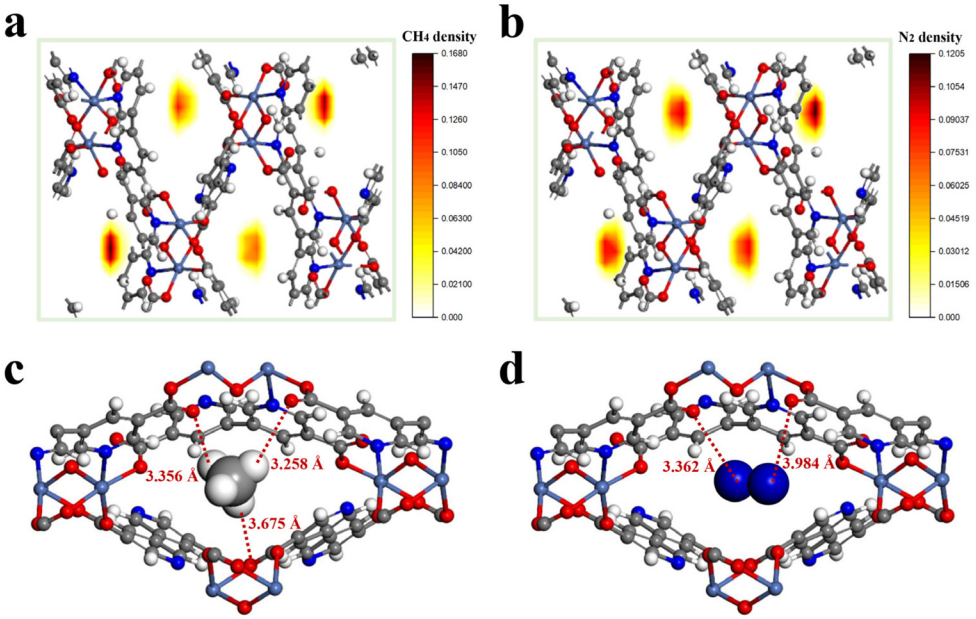

Fig. 3 (a and b) Density distributions of CH_4 and N_2 within TUTJ-201Ni at 298 K, the red dashed circles indicate the favorable adsorption sites. (c and d) The DFT-optimized adsorption configurations of CH_4 and N_2 in TUTJ-201Ni.

Published on 23 May 2024. Downloaded on 15/9/2025 12:27:09 AM.

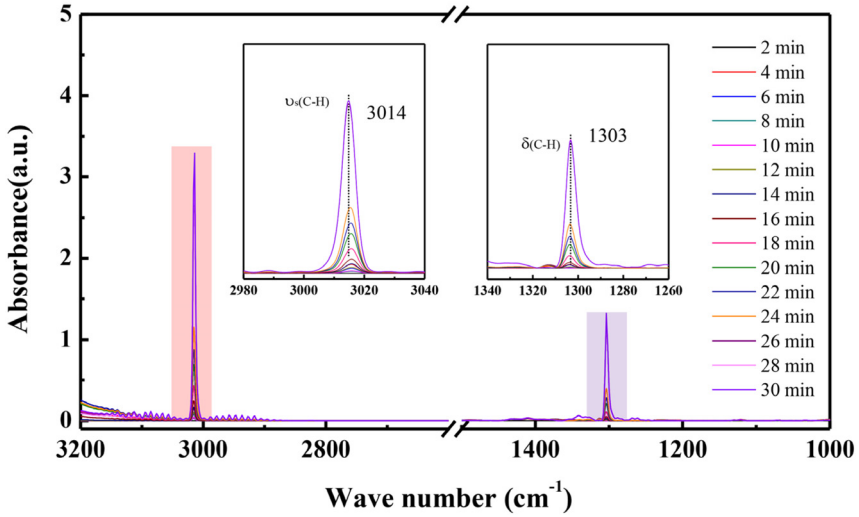

Fig. 4 *In situ* IR spectra of CH_4 adsorbed on TUTJ-201Ni with different CH_4 dosing durations at 298 K.

conducted. As depicted in Fig. 5a, for 50/50 CH_4/N_2 mixtures, N_2 first penetrated the adsorption bed at 1.5 min g^{-1}, and after long periods, CH_4 was detected. The difference between the breakthrough times of the two gases reached 1.4 min g^{-1}, which offers a large operating window for CH_4 release during pressure-swing adsorption processes. Furthermore, eight continuous cycling breakthrough experiments were performed on TUTJ-201Ni. No appreciable change in retention time was observed, proving its good recyclability for CH_4/N_2 separation. After each cycle, TUTJ-201Ni in the column can be readily regenerated within 30 min by He purge. We also investigated the concentration capacity of this material for low concentrations of CH_4 (Fig. 5b); when the CH_4/N_2 ratio was adjusted to 10/90, TUTJ-201Ni still had a good separation effect. Fig. 5c and d show the breakthrough curves under different temperatures or with different flow rates. The results demonstrated that TUTJ-201Ni effectively separates CH_4 from the mixture under various practical separation scenarios.

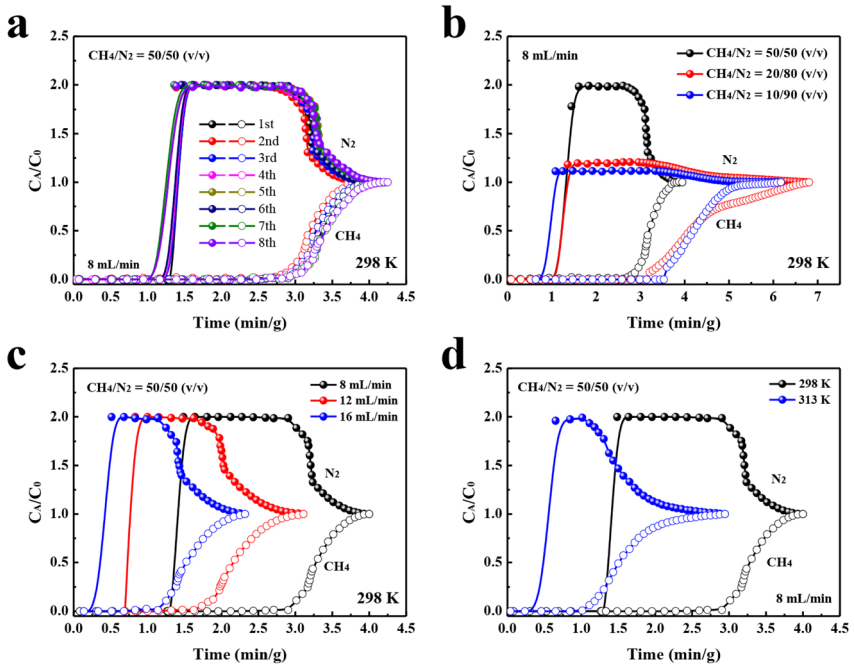

Fig. 5 (a) Experimental breakthrough cycles for CH_4/N_2 (50/50) separation on TUTJ-201Ni at 298 K and 1.0 bar. (b) Experimental breakthrough curves obtained for 50/50, 20/80, and 10/90 mixtures under a flow rate of 8 mL min^{-1} at 298 K and 1.0 bar. (c) Breakthrough curves of TUTJ-201Ni for CH_4/N_2 (50/50) mixtures at 298 K with the flow rate of 8, 12, and 16 mL min^{-1}. (d) Experimental breakthrough curves obtained for TUTJ-201Ni during the separation of CH_4/N_2 (50/50) at 1.0 bar and different temperatures.

 This journal is © the Partner Organisations 2024

Published on 23 May 2024. Downloaded on 15/9/2025 12:27:09 AM.

4. Conclusion

In this study, we developed a novel Ni-based MOF, TUTJ-201Ni, with a high density of accessible oxygen sites for efficient CH_4/N_2 separation. Because of the strong affinity of the CH_4 molecule within the framework, the CH_4/N_2 selectivity of TUTJ-201Ni reaches up to 7.2, along with satisfactory CH_4 uptake (19.8 $cm^3\ g^{-1}$). GCMC simulations combining DFT calculations indicated that two uncoordinated carboxylate oxygen atoms and one μ_2-hydroxyl oxygen atom in the pore wall could selectively combine with the H atoms of the CH_4 molecule *via* multiple C–H···O interactions, thereby affording strong CH_4 adsorption affinity. Breakthrough experiments confirmed that TUTJ-201Ni can separate CH_4/N_2 mixtures under various separation scenarios. Our work not only provides a potential candidate for the separation of CH_4/N_2 in practical industries but also demonstrates the significance of designing oxygen sites for this challenging task.

Author contributions

F. Zhang: methodology, data curation, formal analysis, investigation, writing – original draft. Y. Tang: investigation, data curation. Z. Zhao: investigation, data curation. M. Lu: investigation, data curation. X. Wang: validation, review and editing. J. Li: supervision. J. Yang: review and editing, project administration, funding acquisition. All authors have given approval to the final version of the manuscript.

Conflicts of interest

There are no conflicts of interest to declare.

Acknowledgements

We acknowledge the financial support from the National Natural Science Foundation of China (no. 22378287), the Joint Founds of the National Natural Science Foundation of China (no. U20B6004), the Natural Science Foundation of Shanxi Province (no. 202303021222012) and the Shanxi Research Institute of Huairou Laboratory (no. 202201080301003).

Notes and references

1 D. Saha, H. A. Grappe, A. Chakraborty and G. Orkoulas, Postextraction Separation, On-Board Storage, and Catalytic Conversion of Methane in Natural Gas: A Review, *Chem. Rev.*, 2016, **116**, 11436–11499.

2 Y. Chen, H. Wu, Y. Yuan, D. Lv, Z. Qiao, D. An, X. Wu, H. Liang, Z. Li and Q. Xia, Highly rapid mechanochemical synthesis of a pillar-layer metal-organic framework for efficient CH_4/N_2 separation, *Chem. Eng. J.*, 2020, **385**, 123836.

3 B. Yuan, X. Wu, Y. Chen, J. Huang, H. Luo and S. Deng, Adsorption of CO_2, CH_4, and N_2 on Ordered Mesoporous Carbon: Approach for Greenhouse Gases Capture and Biogas Upgrading, *Environ. Sci. Technol.*, 2013, **47**, 5474–5480.

4 G. Xiao, T. L. Saleman, Y. Zou, G. Li and E. F. May, Nitrogen rejection from methane using dual-reflux pressure swing adsorption with a kinetically-selective adsorbent, *Chem. Eng. J.*, 2019, **372**, 1038–1046.

5 M. Gu, B. Zhang, Z. Qi, Z. Liu, S. Duan, X. Du and X. Xian, Effects of pore structure of granular activated carbons on CH_4 enrichment from CH_4/N_2 by vacuum pressure swing adsorption, *Sep. Purif. Technol.*, 2015, **146**, 213–218.

6 D. M. Ruthven, Past Progress and Future Challenges in Adsorption Research, *Ind. Eng. Chem. Res.*, 2000, **39**, 2127–2131.

7 H. Dai, Q. Zhao, B. Lin, S. He, X. Chen, Y. Zhang, Y. Niu and S. Yin, Premixed combustion of low-concentration coal mine methane with water vapor addition in a two-section porous media burner, *Fuel*, 2018, **213**, 72–82.

8 D. S. Sholl and R. P. Lively, Seven chemical separations to change the world, *Nature*, 2016, **53**, 435–437.

9 H. Wang, Y. Liu and J. Li, Designer Metal-Organic Frameworks for Size-Exclusion-Based Hydrocarbon Separations: Progress and Challenges, *Adv. Mater.*, 2020, **32**, 2002603.

10 J.-R. Li, R. J. Kuppler and H.-C. Zhou, Selective gas adsorption and separation in metal-organic frameworks, *Chem. Soc. Rev.*, 2009, **38**, 1477–1504.

11 R. T. Yang, *Adsorbents: Fundamentals and Applications*, Wiley, Hoboken, 2003.

12 I. A. A. C. Esteves, M. S. S. Lopes, P. M. C. Nunes and J. P. B. Mota, Adsorption of natural gas and biogas components on activated carbon, *Sep. Purif. Technol.*, 2008, **62**, 281–296.

13 J. A. C. Silva, A. Ferreira, P. A. P. Mendes, A. F. Cunha, K. Gleichmann and A. E. Rodrigues, Adsorption Equilibrium and Dynamics of Fixed Bed Adsorption of CH_4/N_2 in Binder less Beads of 5A Zeolite, *Ind. Eng. Chem. Res.*, 2015, **54**, 6390–6399.

14 M. Mofarahi and A. Bakhtyari, Experimental Investigation and Thermodynamic Modeling of CH_4/N_2 Adsorption on Zeolite 13X, *J. Chem. Eng. Data*, 2015, **60**, 683–696.

15 Z. Yang, D. Wang, Z. Menga and Y. Li, Adsorption separation of CH_4/N_2 on modified coal-based carbon molecular sieve, *Sep. Purif. Technol.*, 2019, **218**, 130–137.

16 R.-B. Lin, S. Xiang, W. Zhou and B. Chen, Microporous Metal-Organic Framework Materials for Gas Separation, *Chem*, 2020, **6**, 337–363.

17 L. Li, R.-B. Lin, R. Krishna, H. Li, S. Xiang, H. Wu, J. Li, W. Zhou and B. Chen, Ethane/ethylene separation in a metal-organic framework with iron-peroxo sites, *Science*, 2018, **362**, 443–446.

18 X. Cui, K. Chen, H. Xing, Q. Yang, R. Krishna, Z. Bao, H. Wu, W. Zhou, X. Dong, Y. Han, B. Li, Q. Ren, M. J. Zaworotko and B. Chen, Pore chemistry and size

Published on 23 May 2024. Downloaded on 15/9/2025 12:27:09 AM.

control in hybrid porous materials for acetylene capture from ethylene, *Science*, 2016, **353**, 141–144.
19 H. Furukawa, K. E. Cordova, M. O'Keeffe and O. M. Yaghi, The Chemistry and Applications of Metal-Organic Frameworks, *Science*, 2013, **341**, 1230444.
20 S. B. Peh and D. Zhao, Tying amines down for stable CO_2 capture Sequestering greenhouse gas for different fuel mixes requires better sorbent stability, *Science*, 2020, **369**, 372–373.
21 L. Zhou, P. Brantuas, A. Henrique, H. Reinsch, M. Wahiduzzaman, J.-M. Greneche, A. E. Rodrigues, J. A. C. Silva, G. Maurin and C. Serre, A Microporous Multi-Cage Metal-Organic Framework for an Effective One-Step Separation of Branched Alkanes Feeds, *Angew. Chem.*, 2024, **136**, e202320008.
22 M. Chang, F. Wang, Y. Wei, Q. Yang, J.-X. Wang, D. Liu and J.-F. Chen, Separation of CH_4/N_2 by an ultra-stable metal-organic framework with the highest breakthrough selectivity, *AIChE J.*, 2022, **68**, e17794.
23 Z. Niu, X. Cui, T. Pham, P. C. Lan, H. Xing, K. A. Forrest, L. Wojtas, B. Spacea and S. Ma, A Metal-Organic Framework Based Methane Nano-trap for the Capture of Coal-Mine Methane, *Angew. Chem., Int. Ed.*, 2019, **58**, 10138–10141.
24 S.-M. Wang, M. Shivanna and Q.-Y. Yang, Nickel-Based Metal-Organic Frameworks for Coal-Bed Methane Purification with Record CH_4/N_2 Selectivity, *Angew. Chem., Int. Ed.*, 2022, **61**, e202201017.
25 P. Liu, L. Fan, J. Li, Z. Wu, Y. Wang, Y. Chen, J. Gao, J. Yang, J. Li, B. Chen and L. Li, A Microporous Titanium Metal-Organic Framework with Double Nanotraps for Record CH_4/N_2 Separation, *Chem. Mater.*, 2024, **36**, 2925–2932.
26 Y. Chen, Y. Wang, Y. Wang, Q. Xiong, J. Yang, L. Li, J. Li and B. Mu, Improving CH_4 uptake and CH_4/N_2 separation in pillar-layered metal-organic frameworks using a regulating strategy of interlayer channels, *AIChE J.*, 2022, **68**, e17819.
27 M. Chang, J. Ren, Q. Yang and D. Liu, A robust calcium-based microporous metal-organic framework for efficient CH_4/N_2 separation, *Chem. Eng. J.*, 2021, **408**, 127294.
28 L. Li, L. Yang, J. Wang, Z. Zhang, Q. Yang, Y. Yang, Q. Ren and Z. Bao, Highly efficient separation of methane from nitrogen on a squarate-based metal-organic framework, *AIChE J.*, 2018, **64**, 3681–3689.
29 D. Lv, Y. Wu, J. Chen, Y. Tu, Y. Yuan, H. Wu, Y. Chen, B. Liu, H. Xi, Z. Li and Q. Xia, Improving CH_4/N_2 selectivity within isomeric Al-based MOFs for the highly selective capture of coal-mine methane, *AIChE J.*, 2020, **66**, e16287.
30 M. Chang, Y. Zhao, Q. Yang and D. Liu, Microporous Metal-Organic Frameworks with Hydrophilic and Hydrophobic Pores for Efficient Separation of CH_4/N_2 Mixture, *ACS Omega*, 2019, **4**, 14511–14516.
31 X. Ren, T. Sun, J. Hu and S. Wang, Highly enhanced selectivity for the separation of CH_4 over N_2 on two ultra-microporous frameworks with multiple coordination modes, *Microporous Mesoporous Mater.*, 2014, **186**, 137–145.
32 J. Hu, T. Sun, X. Liu, Y. Guo and S. Wang, Separation of CH_4/N_2 mixtures in metal-organic frameworks with 1D micro-channels, *RSC Adv.*, 2016, **6**, 64039–64046.
33 Z. Huang, P. Hu, J. Liu, F. Shen, Y. Zhang, K. Chai, Y. Ying, C. Kang, Z. Zhang and H. Ji, Enhancing CH_4/N_2 separation performance within aluminum-based Metal-Organic Frameworks: Influence of the pore structure and linker polarity, *Sep. Purif. Technol.*, 2022, **286**, 120446.
34 Q. Shi, J. Wang, H. Shang, H. Bai, Y. Zhao, J. Yang, J. Dong and J. Li, Effective CH_4 enrichment from N_2 by SIM-1 via a strong adsorption potential SOD cage, *Sep. Purif. Technol.*, 2020, **230**, 115850.
35 T. K. N. Phuong, T. D. N. Huong, Q. P. Hung, J. Kim, E. C. Kyle and H. Furukawa, Synthesis and Selective CO_2 Capture Properties of a Series of Hexatopic Linker-Based Metal-Organic Frameworks, *Inorg. Chem.*, 2015, **54**, 10065–10072.

 This journal is © the Partner Organisations 2024